The 9th European Congress on Computational Methods in Applied Sciences and Engineering
ECCOMAS Congress 2024
3–7 June 2024, Lisboa, Portugal

AN INTERSECTION INTERACTION HYBRID METHOD FOR ENERGY FLOW AT MID-HIGH FREQUENCY FOR COMPLEX CAVITIES ACOUSTIC

T. WANGLOMKLANG[1], F. GILLOT[2], AND S. BESSET[1]

[1] LTDS/D2S, École Centrale de Lyon, 36 av. Guy de Collongue,
69134 Ecully Cedex, France,
e-mail: thanasak.wanglomklang@ec-lyon.fr, sebastien.besset@ec-lyon.fr

[2] ELyTMaX IRL3757, CNRS, Univ Lyon, INSA Lyon, Centrale Lyon,
Université Claude Bernard Lyon 1, Tohoku University, Sendai, Japan
e-mail: frederic.gillot@ec-lyon.fr

Key words: Energy Method, Vibro-Acoustic, Mid-High Frequency Range, Ray Tracing, Intersection Algorithm, Energy Density

Summary. We present an efficient way to compute the acoustic energy within complex-shaped geometries and obstacles inside cavities in the mid-high frequency range. The method is based on energy flow, known as the Simplified Energy Method (MES), considered quite accurate in this frequency range. However, its performance is primarily effective in simple cavity shapes and does not adequately address obstacles within the domain. We then propose a hybrid method that couples ray and triangle intersection techniques with the MES formulation. This method involves calculating ray intersection points to identify blocking elements before computing the energy transfer in each boundary element. We rely on a primary intersection state matrix, which contains the overall information of the direct view between elements. This matrix is then integrated into a modified MES equation, thereby disabling unnecessary computation and ensuring precise energy transfer of blind couples. The hybrid formulation is applied to both direct and reverberant fields to calculate the total energy density. Numerical simulations are conducted in a complex domain enclosure and compared with traditional MES calculations and physical properties. The simulation results demonstrated the accuracy of the proposed algorithms, and the computational cost is analyzed and appears to be totally suitable for shape optimization problems, as it usually involves many 'call' of the objective function.

1 INTRODUCTION

In the framework aimed at enhancing acoustic performance across various environments, from transportation compartments like aircraft cabins, cars, and boats to building rooms, the reduction of noise levels holds paramount importance. Typically, pressure noise exhibits three distinct behaviors as frequency increases. The first band describes the low-frequency region, where methods such as finite element methods (FEM) and boundary element methods (BEM) are well-suited [1]. The second and third frequency regions define the mid and high frequency domains, characterized by high modal density. The primary challenge at high frequencies lies in managing small wavelengths, necessitating the handling of numerous degrees of freedom. Several

studies have indicated that deterministic techniques such as the FEM and BEM encounter challenges when processing the extensive datasets needed, especially when addressing the mid-high frequency range, proving computationally intensive for large models [2]. Over the past decade, a method based on geometrical acoustics has been applied to address this frequency band. The image-source method uses virtual sound sources to simulate sound reflection off surfaces, based on the assumption of sound traveling in straight lines with specular reflections from opposing surfaces. [3]. In contrast, ray tracing involves simulating sound propagation as a series of rays emitted from a source. As these ray encounter surfaces, they are absorbed, reflected, or transmitted based on the acoustic properties of the materials they encounter [4]. For enclosures, both the image-source method and ray tracing can be applied efficiently [5]. However, their significant computational demands, particularly in complex environments, limit their practicality for large-scale or highly detailed applications [6]. Advanced techniques such as Statistical Energy Analysis (SEA) for vibroacoustic are also of interest for medium and high frequency acoustic analysis. SEA has been applied with considerable success, leveraging the consideration of mechanical energy within complex-built structures [7, 8]. The system is divided into subsystems, with energy exchange defined based on the statistical coupling of subsystem modes. Several researchers have studied the application of SEA in acoustic simulation. For instance, authors in [9] utilized the SEA model to estimate the sound pressure level generated by a commercial refrigerator in a reverberant field, defining 26 subsystems with parameters necessary for model computation, such as modal density, bending wave speed, bending wave number, bending wavelength, damping loss factor, and critical frequency. Their results were compared against real-world experiments. Cordioli et al. [10] explored the efficacy of SEA in vibro-acoustic vehicle modeling, demonstrating its usefulness in preemptively addressing noise issues and optimizing noise control from the design phase. Additionally, Shorter, P. J., and Langley, R. S. [11] reviewed the integration of SEA with other numerical methods for analyzing vibro-acoustic interactions in complex systems, with numerous developments and applications documented in references [12, 13, 14]. Energy methods provide efficient alternatives for high and medium frequency ranges, where numerical approaches such as FEA or BEM formulations become computationally intensive. In contrast to these methods, which require fine meshes, energy methods can yield results within seconds or minutes, significantly reducing computational time. In this work focuses on a local energy formulation for acoustic cavities. The initial development of this method, presented by Nefske and Sung [15], extended SEA densities to a local energy formulation for predicting the spatial spread of energy density within subsystems. Subsequent authors have further refined this into the Simplified Energy Method (MES) [16, 17, 23]. MES has been applied across various domains, including beams, membranes, and plates [18, 19, 20, 21, 22], as well as in enclosure acoustic cavities for sound source identification [24], and as an objective function in topology and shape optimization contexts [25, 26]. However, its effectiveness is predominantly limited to simple cavity shapes and struggles to adequately handle obstacles within the domain.

This paper propose a novel method implemented within the MES formulation, enabling its application to more complex acoustic cavities, even in the presence of obstacles within the domain. The technique we propose is based on employing ray and triangle intersection to detect blind couples between elements presented in the matrix, which is then integrated into the modified MES formulation. The present paper is organized as follows: the first part recalls the basic construction of the Simplified Energy Method, then the derivation and adaptation of

ray and triangle intersection algorithms into the MES formulation. Numerical experiments are provided in this study. The validation of the new approach utilizes the energy conservation law to investigate the total energy transfer in the enclosure cavity. Finally, the results were achieved by comparing the proposed method with conventional MES in cases of complex acoustic cavities, including those with internal obstacles.

2 SIMPLIFIED ENERGY METHOD (MES)

2.1 General description of MES

The principle of the Simplified Energy Method is based on determining the energy density W and the energy flow $\mathbf{I}$ resulting from source in a domain Ω with the boundary $\partial\Omega$ Illustrated in in Figure 1, radiation energy at point M is computed in two forms: firstly, the direct field energy emitted by the primary source at S and secondly, the fictitious or reverberating energy transmitted from the surface boundary defined as element dP. This study focuses on the steady-state equation; hence, the numerical implementation for the transient state has not been addressed.

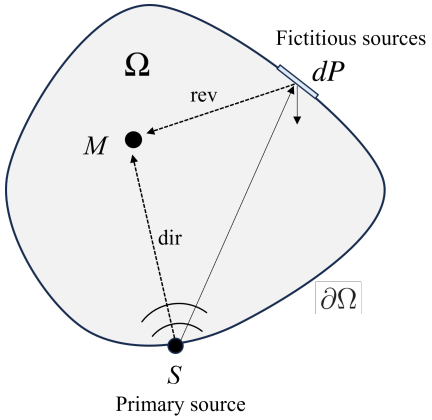

Figure 1: Energy transfer from direct and reverberated fields to a specific point M

The initial step involves an energy balance to describe the local energy quantity at the observation point M, expressed as follows:

$$-\nabla\vec{\mathbf{I}} = \pi_{\text{diss}} \tag{1}$$

Here, ∇ represents the gradient operator, π_{diss} denotes the power dissipation. The dissipation power term is analogous to that found in the SEA viscous model, as previously discussed in literature references [5, 7], which describes $\pi_{\text{diss}} = \eta\omega W$ where η is the damping loss factor, assumed to be minimal in acoustic fluids, and ω is the angular frequency. The MES method incorporates waves that consist of both direct and reverberated energy components. The direct field results from the input power source, while the reverberated field emerges from boundary reflections [24]. This paper focuses specifically on the energy density W, which is related to the square of the sound pressure in the cavity. By considering both fields, we apply the superposition principle:

$$W = W_{\text{dir}} + W_{\text{rev}} \tag{2}$$

The relationship between the propagative waves, energy flow, and energy density is notably straightforward. Utilizing an intrinsic energy law, we define wave velocity c as follows [25]:

$$\vec{\mathbf{I}}(M) = cW(M)\vec{\mathbf{n}} \tag{3}$$

Where $\vec{\mathbf{n}}$ is the unit vector directed towards observation point M. In a 3D space, the wave fields are symmetrical about the source point S. The propagation fields vary with the distance r form S to M. Thus, we can reformulate the energy balance equations (1) and (3) as:

$$\frac{1}{r^2}\frac{\partial}{\partial r}(r^2\vec{\mathbf{I}}) = 0 \tag{4}$$

Where r is the distance from the source point S to the observation point M. Equation (4) can be rewrited by focusing on the energy density in the W field:

$$-c^2\frac{1}{r^2}\frac{\partial}{\partial r}(r^2W\vec{\mathbf{n}}) = 0 \tag{5}$$

Equation (5) is termed the *local energy equation* for symmetrical wave propagation, a concept central to the radiosity method. This method, initially proposed by Kuttruff [27], is the focus of our current approach. To derive solutions for equations (4) and (5), we introduce elementary expressions: $G(r)$ for energy density and $\mathbf{H}(r)$ for energy flow, under analogous conditions, represented as:

$$G(r) = \frac{1}{\gamma_0 cr^2} \quad \text{and} \quad \mathbf{H}(r) = \frac{1}{\gamma_0 r^2}\vec{\mathbf{u}_r} \tag{6}$$

Where γ_0 denotes the solid angle of the space under consideration ($\gamma_0 = 4\pi$) in a three dimensional space and $\vec{\mathbf{u}_r}$ represents the unit vector from the source, covering both direct and reverberated fields, to the observation point M.Utilizing the principle of superposition for energy, the combined energy fields of energy density and energy flow within the cavity are modeled based on the contribution from primary sources and fictitious sources, the latter representing unknown parameters of the reverberant field. The formalization of these energy fields is provided in the representation formulas that:

$$W(M) = \int_\Omega \rho(S)G(S,M)\,dS + \int_{\partial\Omega} \sigma(P,\theta_P)G(P,M)\,dP \tag{7}$$

$$\mathbf{I}(M) = \int_\Omega \rho(S)\mathbf{H}(S,M)\,dS + \int_{\partial\Omega} \sigma(P,\theta_P)\mathbf{H}(P,M)\,dP \tag{8}$$

Where ρ is the intensity of the primary source, which is a known quantity, and σ is the magnitude of the fictitious sources that need to be determined. To achieve this, we describe the secondary source, which varies with the angle θ_P (see Figure 2). This concept is commonly known as the law of perfectly diffuse reflection (Lambert's law of cosine emission direction). The boundary sources $\sigma(P)$ serve as the unknowns we aim to determine in the problem. These sources account for the reverberated energy and are calculated by considering the energy balance at the boundary interfaces. We establish the power balance by introducing the absorption coefficient α , which is the ratio of the reflected power to the incident power (ranging from 0 to 1), observed at a point P. Therefore, the total reflected energy can be characterized as follows:

$$\sigma(P) = (1-\alpha)\left(\int_\Omega \rho(S)\mathbf{H}(S,P)\,dS + \int_{\partial\Omega} 4\cos(\theta_Q)\sigma(Q)\mathbf{H}(Q,P)\,dQ\right)\cdot\vec{\mathbf{n}}_P \tag{9}$$

Where $\vec{\mathbf{n}}_P$ is the outward normal vector at point P. This form of the integral equation is termed the Fredholm equation of the second kind, with $\sigma(P)$ as the unknowns. To solve this, we will implement a discretization strategy for the structure and a standard numerical scheme, details of which will be provided later.

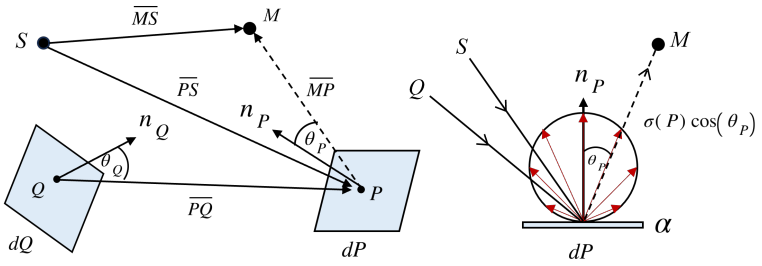

Figure 2: Notation of interaction from source to element and element to element.

2.2 Implementation of the Simplified Energy Method (MES)

This section is devoted to detailing the numerical implementation of MES. The foundation of this implementation is the matrix operator T, which operates within the function space defined on the boundary $\partial\Omega$. This operator is integral to addressing the boundary sources as specified in equation (9):

$$T : \sigma \to (1-\alpha) \int_{\partial\Omega} \sigma(Q) \underbrace{V(Q,P) \cdot \frac{\cos(\theta_Q)\cos(\theta_P)}{\pi |PQ|^2} \, dQ}_{\text{Kernel } K} \tag{10}$$

To facilitate the integration process and to account for obstacles that may block the line of sight, we introduce a binary visibility coefficient $V(Q,P)$ which is essential for assessing the potential energy exchange between two boundary surfaces. According to the principle of energy conservation within an enclosure, the integration over the kernel K, ensuring that the total energy interacting with a point on the boundary sums up to unity. This principle can be applied for validating the numerical calculation in the paper which will be provided in the numerical experiment. Based on equation (9), this can thus be written in matrix form where I_d represents the identity operator:

$$(I_d - T)\sigma(P) = B(P) \tag{11}$$

The right-hand side B corresponds to the contributions from primary sources which construct the elementary $\mathbf{H}$ defined by:

$$B(P) = (1-\alpha) \int_{\Omega} V(S,P) \cdot \frac{\cos(\theta_P)}{4\pi |SP|^2} \, dS \tag{12}$$

The numerical implementation can be performed through boundary discretization. The reverberating fields will be solved by equation (11) which is: $\sigma(P) = (I_d - T)^{-1} B(P)$ then the final energy density referred to in equation (7) can be expressed:

$$W(M) = \sum_{k=1}^{N_k} \frac{\rho(S)_k}{4\pi c |S_k M|^2} \cdot V(S_k, M) + \sum_{j=1}^{N_j} \frac{\sigma(P_j)\cos(\theta_{P_j})}{\pi c |P_j M|^2} \cdot V(P_j, M) \tag{13}$$

In equation (13), k represents the count of primary sources, and j indexes the boundary elements. It is also crucial to note that inside the boundary $\partial\Omega$, there may be complex geometries or obstructions that could interfere with the energy paths between points P and Q. The next section will introduce the computation of the visibility coefficient matrix V, which significantly improves the accuracy of energy transfer calculations throughout the acoustic domain we are analyzing.

3 HYBRID METHOD FOR MES IN COMPLEX CAVITY

In the previous section, we discussed the MES formulation and its numerical application. Our primary focus now is to introduce a method that enables the application of MES in more complex cavity shapes, even in the presence of internal obstacles. This hybrid method incorporates ray and triangle intersection algorithms, as presented by Möller, T. [28]. As illustrated in Figure 3, we discretize the acoustic cavity into a mesh of triangles, with the center of each mesh element pair represented by points O and S.

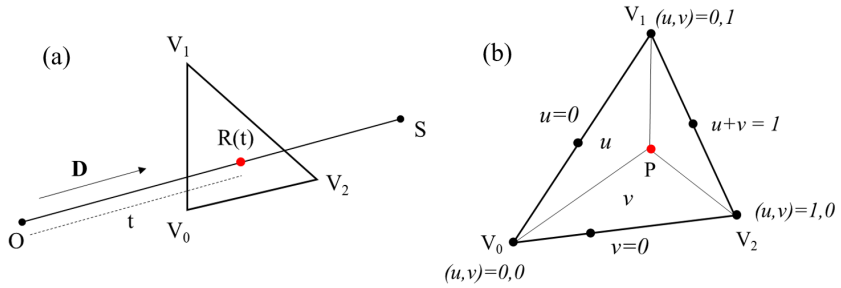

Figure 3: illustrates two key concepts: (a) the intersection of a ray with a triangle and (b) the criteria for the movement of the intersection point within barycentric coordinates.

The direction vector D is determined by the relative positions of the element pairs, using the vertices V_0, V_1 and V_2 of the blocking element (obstacle). The intersection point is represented by a parametric ray equation:

$$R(t) = O + tD \tag{14}$$

Where t is a scalar that represents the distance along the ray from the originating element O to the potential intersection point on the obstructing triangle. To describe a point P on the plane of the triangle, we employ barycentric coordinates with the parameters u and v, utilizing the vertices of the triangle. This approach is applied to validate whether a sound ray intersects with a triangle, which is essential for understanding sound propagation in complex environments. A point P on the triangle is thus expressed in barycentric coordinates as:

$$P(u, v) = (1 - u - v)V_0 + uV_1 + vV_2 \tag{15}$$

From equation (15), point P is located inside the triangle if $u \geq 0, v \geq 0$, and $u + v \leq 1$. The intersection between the ray $R(t)$ and the triangle at point $P(u, v)$ occurs when these conditions are satisfied, leading to the equation:

$$O + tD = (1 - u - v)V_0 + uV_1 + vV_2 \tag{16}$$

Rearranging the terms, we obtain:

$$\begin{bmatrix} -D, & V_1 - V_0, & V_2 - V_0 \end{bmatrix} \begin{bmatrix} t \\ u \\ v \end{bmatrix} = O - V_0 \tag{17}$$

Equation (17) can be geometrically interpreted by mapping to the x, y and z coordinate and is solvable using Cramer's rule:

$$\begin{bmatrix} t \\ u \\ v \end{bmatrix} = \begin{bmatrix} T & E_1 & E_2 \\ -D & T & E_2 \\ -D & E_1 & T \end{bmatrix}^{-1} \tag{18}$$

Where $E_1 = V_1 - V_0$, $E_2 = V_2 - V_0$ and $T = O - V_0$. By solving Equation (24), we can identify which elements between paired considerations create an obstacle by presenting more than one intersection point for each ray direction. A value of 0 is assigned when intersections are found, and a value of 1 when they are present. This binary assignment is then integrated into the visibility matrix V, which is essential in the MES formulation, particularly for complex acoustic scenarios.

4 NUMERICAL SIMULATIONS

4.1 Verification of the Hybrid Method

This section details a numerical simulation conducted for a complex acoustic cavity to validate our proposed method. The cavity has a rectangular shape with dimensions is 4×6×3 m. We assume that all boundaries have an absorption coefficient of 0.5. A point source, emitting 1 W of power and located at 5.5, 2, 0.8 m within the cavity. Inside, there are two obstacles, both subject to the same conditions depicted in Figure 4. The entire cavity is discretized into a triangular mesh consisting of 400 elements using Gmsh software, an open-source tool that is adept at creating and meshing finite element models. The mesh elements generated in Gmsh are exported in the .VTK file format, which is compatible with Python. For the acoustic simulations in this research, we utilize the PyVista API in Python to manage the mesh data effectively. The validation of the hybrid method will be examined.

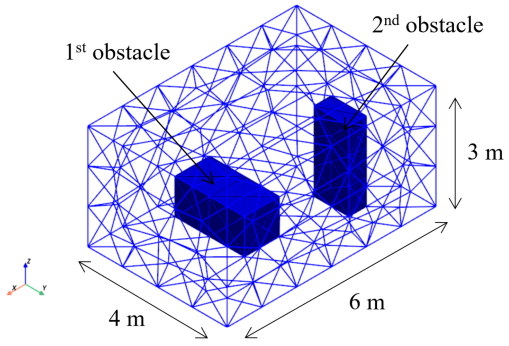

Figure 4: The acoustic cavity finite element domain.

To execute the obstacle checking algorithm, we can employ the principle that calculates the sum of the energy fractions exchanged by a patch within an enclosed cavity as referred to in equation (10). The numerical method to compute this is the well-known contour integration method presented in [29]. The result in Figure 5 demonstrates the conservation of energy across each element. It is apparent that the obstacle check algorithm plays a crucial role in the accuracy of energy exchange calculations within the acoustic domain. Calculations performed without obstacle checking (represented by the red data points) show a significant deviation from the ideal value. This variance not only indicates a less accurate energy exchange assessment but also highlights the potential for overestimation of the energy transfer in scenarios where the sound waves are obstructed. Contrastingly, when obstacle checking is applied (indicated by the black data points), the sum of the form vectors consistently approaches the ideal value of 1.

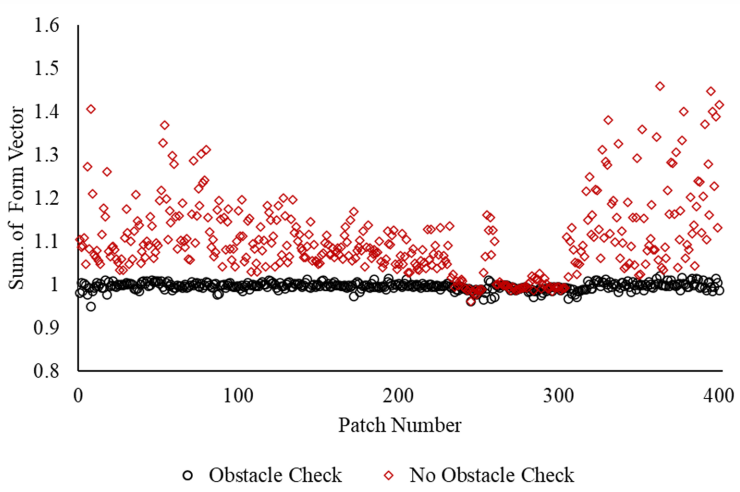

Figure 5: The result of summation from vector, comparison between using obstacle check algorithm (black) and calculation without obstacle checking (red).

4.2 Numerical result of Sound Pressure Level (SPL)

The comparison of sound behavior is provided by examining two distinct acoustic cavities: a simple rectangular cavity and a more complex configuration with two obstacles, comparing their acoustic responses. The sound pressure level (SPL), measured in decibels (dB), was used to gauge energy density within these spaces. To examine sound movement, we measured SPLs across two planes: the XY plane, situated 0.5 meters from the base, and the XZ plane, 1.5 meters from the left side wall. As expected, and depicted in Figure 6(a), the SPL within the unobstructed cavity showed a reduction in a spherical pattern moving away from the source. This observation aligns with the inverse square law, which states that sound intensity decreases as the distance from the source increases. Additionally, we observed the influence of sound waves reflecting off the cavity boundary, creating a reverberation effect. The highest SPL recorded was 122 dB near the source, tapering to a minimum of 112 dB at the furthest measured points. In contrast, the complex cavity scenario presented in Figure 6(b) demonstrated the significant impact of obstructions on sound distribution. The presence of obstacles not only disrupted the

direct path of sound waves but also affected the reverberation patterns, creating areas of lower SPL behind them. Notably, the lowest SPL recorded at a comparable position to the open cavity was 106 dB, found behind the second obstacle. These findings reveal that obstructions within an acoustic space can lead to considerable variations in SPL distribution. This is a crucial consideration for real-world applications, such as in the optimization design of acoustic cavity shapes and includes the analysis of the effects of changing absorption coefficients, which can present uncertainty in design. In the subsequent section, we will delve into the effects of varying absorption coefficients. By adjusting these coefficients, we aim to explore how different materials within the cavity affect the SPL distribution.

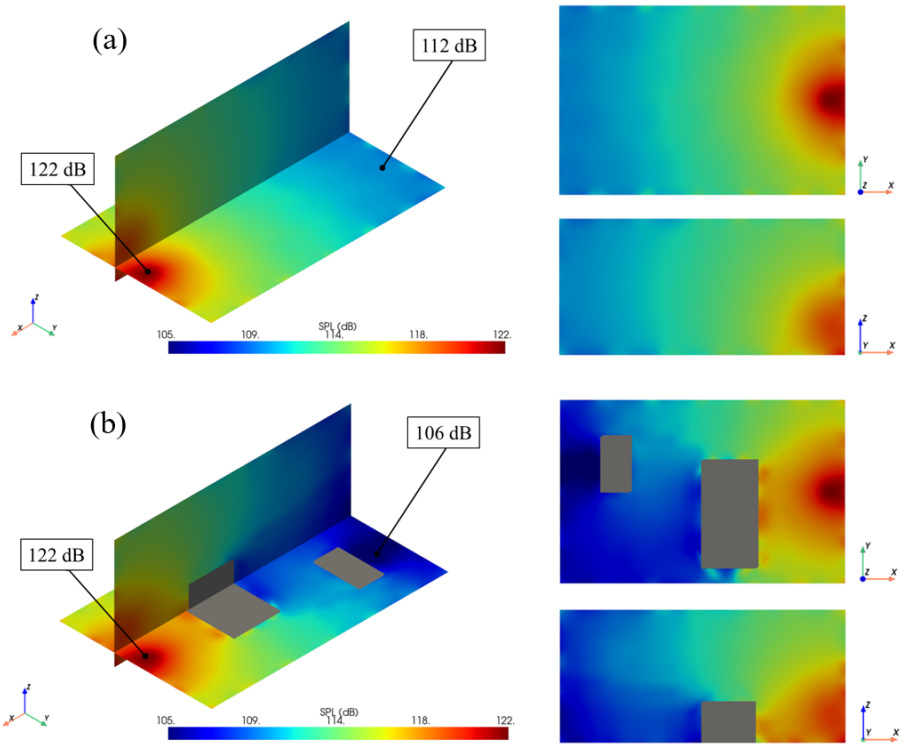

Figure 6: Sound pressure map in a cavity excited by a point source. (a) no obstacle (b) with obstacle.

The provided figures, Figures 7 illustrate the effects of varying absorption coefficients on the sound pressure level (SPL) in an acoustic cavity with obstacles. The dashed line indicates the measurement direction for SPL across a section of the cavity, and the absorption coefficients are varied in the simulation by 0.3, 0.5 and 0.7 replectively. These results suggest that as the absorption coefficient increases, the SPL within the cavity decreases, which is consistent with the expectation that more sound energy is absorbed by the surfaces, and less is available to propagate within the space. Absorption coefficients can be strategically placed to reduce reverberation and create areas with significantly lower sound levels as indicated by the areas of lower SPL behind the obstacles. Conversely, for spaces where a certain level of reverberation is desired, materials with lower absorption coefficients might be preferred.

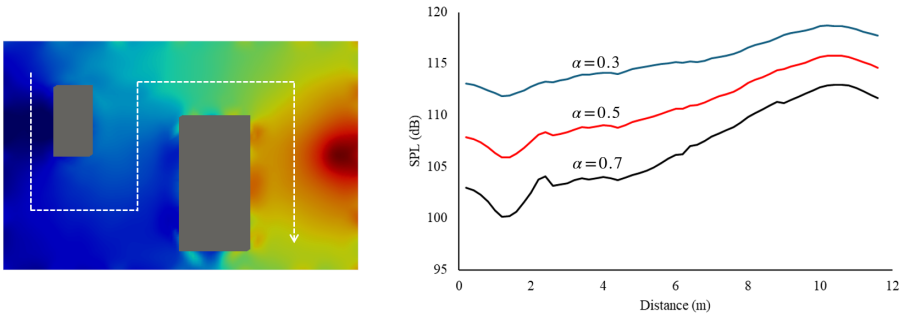

Figure 7: Sound Pressure Level (SPL) Variation with Absorption Coefficients of 0.3 (Blue), 0.5 (Red), and 0.7 (Black)

5 CONCLUSIONS

In the study presented, we have developed a hybrid acoustic energy calculation method that combines ray and triangle intersection techniques with the Simplified Energy Method (MES) to address the challenges of complex shape cavities with internal obstacles. The proposed approach significantly improves the accuracy of the MES, especially in mid-high frequency ranges, by eliminating unnecessary computations for obstructed element pairs. The efficiency and accuracy of the method were validated through numerical simulations, which also demonstrated its superiority over traditional MES in complex acoustic scenarios. The introduction of a primary intersection state matrix was crucial in achieving precise energy transfer, confirming the method potential for intricate geometries. This makes it particularly suitable for applications involving to the shape optimization. The hybrid MES method marks a significant step forward in computational acoustics, providing a refined, computationally feasible tool leveraged to integrate into comprehensive acoustic optimization frameworks.

Acknowledgments

The authors extend sincere thanks to Campus France and the French Government for their scholarship, enabling this research. Appreciation is due to the Mechatronic Engineering Program at Suranaree University of Technology for educational support. Additionally, we are grateful to CNRS (ELyTMax, IRL3757) for their financial backing and research facilitation.

REFERENCES

[1] Łodygowski, T., and W. Sumelka. 2006. “Limitations in Application of Finite Element Method in Acoustic Numerical Simulation.” Journal of Theoretical and Applied Mechanics 44, no. 4: 849–865.

[2] Nosal, E. M., M. Hodgson, and I. Ashdown. 2004. “Investigation of the Validity of Radiosity for Sound-Field Prediction in Cubic Rooms.” The Journal of the Acoustical Society of America 116, no. 6: 3505–3514.

[3] Allen, J. B., and D. A. Berkley. 1979. “Image Method for Efficiently Simulating Small-Room Acoustics.” The Journal of the Acoustical Society of America 65, no. 4: 943–950.

[4] Vorländer, M. 1989. “Simulation of the Transient and Steady-State Sound Propagation in Rooms Using a New Combined Ray-Tracing/Image-Source Algorithm.” The Journal of the Acoustical Society of America 86, no. 1: 172–178.

[5] Le Bot, A., and A. Bocquillet. 2000. “Comparison of an Integral Equation on Energy and the Ray-Tracing Technique in Room Acoustics.” The Journal of the Acoustical Society of America 108, no. 4: 1732–1740.

[6] Savioja, L., and U. P. Svensson. 2015. “Overview of Geometrical Room Acoustic Modeling Techniques.” The Journal of the Acoustical Society of America 138, no. 2: 708–730.

[7] Le Bot, A. 1998. “A Vibroacoustic Model for High Frequency Analysis.” Journal of Sound and Vibration 211, no. 4: 537–554.

[8] Lyon, R. H. 1975. Statistical Energy Analysis of Dynamical Systems Theory and Application. Cambridge, MA: MIT Press.

[9] Zárate, R., J. Poblet-Puig, M. Ortega, and M. López-Parra. 2020. “Statistical Energy Analysis Model for Sound Pressure Level Prediction on Refrigerators.” Acoustics Australia 48: 233–250.

[10] Cordioli, J. A., M. Trichês, and S. N. Gerges. 2004. “Applications of the Statistical Energy Analysis to Vibro-Acoustic Modeling of Vehicles.” SAE Technical Paper 2004-01-3352.

[11] Shorter, P. J., and R. S. Langley. 2005. “Vibro-Acoustic Analysis of Complex Systems.” Journal of Sound and Vibration 288, no. 3: 669–699.

[12] Le Bot, A. 2016. “Applications of SEA in Structural Acoustics.” Journal of Sound and Vibration 363: 385–400.

[13] Brunskog, J. 2012. “Energy Based Prediction Models for Building Acoustics.” In Joint Baltic-Nordic Acoustics Meeting 2012.

[14] Charpentier, A., P. Sreedhar, J. Cordioli, and K. Fukui. 2008. “Modeling Process and Validation of Hybrid FE-SEA Method to Structure-Borne Noise Paths in a Trimmed Automotive Vehicle.” SAE Technical Paper 2008-36-0574.

[15] Nefske, D. J., and S. H. Sung. 1989. “Power Flow Finite Element Analysis of Dynamic Systems: Basic Theory and Application to Beams.”

[16] Le Bot, A. 2002. “Energy Transfer for High Frequencies in Built-Up Structures.” Journal of Sound and Vibration 250, no. 2: 247–275.

[17] Ichchou, M. N., and L. Jezequel. 1996. “Comments on Simple Models of the Energy Flow in Vibrating Membranes and on Simple Models of the Energetics of Transversely Vibrating Plates.” Journal of Sound and Vibration 195, no. 4: 679–685.

[18] Lase, Y., M. N. Ichchou, and L. Jezequel. 1996. “Energy Flow Analysis of Bars and Beams: Theoretical Formulations.” Journal of Sound and Vibration 192, no. 1: 281–305.

[19] Wang, A., N. Vlahopoulos, and K. Wu. 2004. "Development of an Energy Boundary Element Formulation for Computing High-Frequency Sound Radiation from Incoherent Intensity Boundary Conditions." Journal of Sound and Vibration 278, no. 1-2: 413–436.

[20] Bouthier, O. M., and R. J. Bernhard. 1995. "Simple Models of Energy Flow in Vibrating Membranes." Journal of Sound and Vibration 182, no. 1: 129–147.

[21] Hardy, P., M. N. Ichchou, L. Jezequel, and D. Trentin. 2009. "A Hybrid Local Energy Formulation for Plates Mid-Frequency Flexural Vibrations." European Journal of Mechanics-A/Solids 28, no. 1: 121–130.

[22] Houillon, L., M. N. Ichchou, and L. Jezequel. 2005. "Wave Motion in Thin-Walled Structures." Journal of Sound and Vibration 281, no. 3-5: 483–507.

[23] Besset, S., M. N. Ichchou, and L. Jezequel. 2010. "A Coupled BEM and Energy Flow Method for Mid-High Frequency Internal Acoustic." Journal of Computational Acoustics 18, no. 1: 69–85.

[24] Chabchoub, M., S. Besset, and M. N. Ichchou. 2011. "Identification of Acoustic Sources Through an Inverse Energy Method." Inverse Problems in Science and Engineering 19, no. 7: 903–919.

[25] Besset, S., and M. N. Ichchou. 2011. "Acoustic Absorption Material Optimisation in the Mid–High Frequency Range." Applied Acoustics 72, no. 9: 632–638.

[26] Troian, R., S. Besset, and F. Gillot. 2014. "Shape Optimization Under Vibroacoustic Criteria in the Mid-High Frequency Range." Journal of Computational Acoustics 22, no. 2: 1450003.

[27] Kuttruff, H. 1997. "Energetic Sound Propagation in Rooms." Acta Acustica united with Acustica 83, no. 4: 622–628.

[28] Möller, T., and B. Trumbore. 2005. "Fast, Minimum Storage Ray/Triangle Intersection." In ACM SIGGRAPH 2005 Courses, 7–es.

[29] Mazumder, S., and M. Ravishankar. 2012. "General Procedure for Calculation of Diffuse View Factors Between Arbitrary Planar Polygons." International Journal of Heat and Mass Transfer 55, no. 23-24: 7330–7335.